Characterization of a Large Subunit Catalase Truncated by Proteolytic Cleavage[†,‡]

Prashen Chelikani,[§] Xavier Carpena,[§] Rosa Perez-Luque,[||] Lynda J. Donald,[⊥] Harry W. Duckworth,[⊥] Jacek Switala,[§] Ignacio Fita,[||] and Peter C. Loewen*[,§]

Department of Microbiology, University of Manitoba, Winnipeg, Manitoba R3T 2N2, Canada, Consejo Superior de Investigacione Cientificas, Parc Cientific, Josep Samitier 1−5, 08028 Barcelona, Spain, and Department of Chemistry, University of Manitoba, Winnipeg, Manitoba R3T 2N2, Canada

Received December 28, 2004; Revised Manuscript Received February 9, 2005

ABSTRACT: The large subunit catalase HPII from *Escherichia coli* can be truncated by proteolysis to a structure similar to small subunit catalases. Mass spectrometry analysis indicates that there is some heterogeneity in the precise cleavage sites, but approximately 74 N-terminal residues, 189 C-terminal residues, and a 9−11-residue internal fragment, including residues 298−308, are removed. Crystal structure refinement at 2.8 Å reveals that the tertiary and quaternary structure of the native enzyme is retained with only very subtle changes despite the loss of 36% of the sequence. The truncated variant exhibits a 1.8 times faster turnover rate and enhanced sensitivity to high concentrations of H_2O_2, consistent with easier access of the substrate to the active site. In addition, the truncated variant is more sensitive to inhibition, particularly by reagents such as aminotriazole and azide which are larger than substrate H_2O_2. The main channel leading to the heme cavity is largely unaffected by the truncation, but the lateral channel is shortened and its entrance widened by removal of the C-terminal domain, providing an explanation for easier access to the active site. Opening of the entrance to the lateral channel also opens the putative NADPH binding site, but NADPH binding could not be demonstrated. Despite the lack of bound NADPH, the compound I species of both native and truncated HPII are reduced back to the resting state with compound II being evident in the absorbance spectrum only of the heme *b*-containing H392A variant.

Catalases protect organisms against damage from H_2O_2 and its degradation products by degrading hydrogen peroxide to water and oxygen (reaction 1) (*1*)

$$2H_2O_2 \rightarrow 2H_2O + O_2 \quad (1)$$

The reaction takes place in two steps, both involving two-electron transfers, and can involve either a heme or a dimanganese cluster in the reactive center. In heme catalases, the heme is first oxidized by H_2O_2 to an oxoferryl porphyrin cation radical species or compound I (reaction 2) and then reduced by the second H_2O_2 to regenerate the resting (ferric) enzyme, water, and molecular oxygen (reaction 3). In the presence of low H_2O_2 concentrations or one-electron donors, compound I of some catalases can undergo a one-electron reduction to a species called compound II (reaction 4).

$$\text{Enz (Por}-\text{Fe}^{\text{III}}) + H_2O_2 \rightarrow \text{Cpd I (Por}^{+\bullet}-\text{Fe}^{\text{IV}}{=}\text{O}) + H_2O \quad (2)$$

$$\text{Cpd I (Por}^{+\bullet}-\text{Fe}^{\text{IV}}{=}\text{O}) + H_2O_2 \rightarrow \text{Enz (Por}-\text{Fe}^{\text{III}}) + H_2O + O_2 \quad (3)$$

$$\text{Cpd I (Por}^{+\bullet}-\text{Fe}^{\text{IV}}{=}\text{O}) + e^- \rightarrow \text{Cpd II (Por}-\text{Fe}^{\text{IV}}{=}\text{O}) \quad (4)$$

In Mn-containing catalases, the oxidation and reduction steps (reactions 5 and 6) can occur in either order because the two oxidation states of the dimanganese cluster appear to be equally stable.

$$H_2O_2 + \text{Mn}^{\text{II}}-\text{Mn}^{\text{II}}(2H^+) \rightarrow \text{Mn}^{\text{III}}-\text{Mn}^{\text{III}} + 2H_2O \quad (5)$$

$$H_2O_2 + \text{Mn}^{\text{III}}-\text{Mn}^{\text{III}} \rightarrow \text{Mn}^{\text{II}}-\text{Mn}^{\text{II}}(2H^+) + O_2 \quad (6)$$

The catalase reaction has evolved in three phylogenetically unrelated protein types, including the heme-containing monofunctional catalase, the heme-containing bifunctional catalase-peroxidase, and the Mn-containing catalase (*1*). The most widespread and extensively characterized class is the monofunctional catalases, first reported in 1900, which have evolved in three phylogenetically distinct groups or clades, two with small subunits, 55−60 kDa, and one with large subunits, 78−84 kDa (*2*, *3*). At least one representative structure from each clade can be found among the 11

[†] This work was supported by Grant OGP9600 from the Natural Sciences and Engineering Research Council of Canada (to P.L.), by the Canadian Research Chair Program (to P.L.), by a fellowship from the Manitoba Health Research Council (to P.C.), and by Fellowship EX-2003-0866 from the Ministerio de Educación Cultura y Deporte, Spain (to X.C.).

[‡] Structure factors and coordinates have been submitted to the Protein Data Bank as entry 1YE9.

* To whom correspondence should be addressed: Department of Microbiology, University of Manitoba, Winnipeg, MB R3T 2N2, Canada. Phone: (204) 474-8334. Fax: (204) 474-7603. E-mail: peter_loewen@umanitoba.ca.

[§] Department of Microbiology, University of Manitoba.

[||] Consejo Superior de Investigacione Cientifícas.

[⊥] Department of Chemistry, University of Manitoba.

10.1021/bi047277m CCC: $30.25
Published on Web 03/25/2005

monofunctional catalase crystal structures so far determined, including the enzymes from bovine liver (*4*, *5*), *Penicillium vitale* (*6*, *7*), *Micrococcus lysodeikticus* (*8*), *Proteus mirabilis* (9), *Escherichia coli* (*10*, *11*), *Saccharomyces cerevisiae* (*12*, *13*), human erythrocytes (*14*, *15*), *Pseudomonas syringae* (*16*, *17*), *Helicobacter pylori* (*18*), *Neurospora crassa* (*19*), and *Enterococcus faecalis* (*20*).

The large subunit, clade 2 catalase HPII[1] from *E. coli*, has been extensively characterized physically, kinetically, and structurally (*1*). Among its unusual properties, the enhanced resistance to denaturation (*21*) and proteolytic cleavage (*22*) were initially attributed to the interweaving of the 80 N-terminal residues of one subunit through a loop on an adjacent subunit (*21*). However, removal of 75 N-terminal residues did not significantly reduce the thermal stability of the enzyme, whereas removal of the 150-residue C-terminal domain lowered the T_m for loss of activity by 25 °C (*22*), suggesting that the C-terminal domain played a more important role than the N-terminal domain in enzyme stability. Surprisingly, HPII truncated at both the N- and C-terminal ends was resistant to further proteolytic degradation and seemed to retain its quaternary integrity and enzymatic activity. In this paper, we report the biochemical and structural characterization of proteolyzed HPII, confirming that the large subunit HPII can be truncated to a core structure that is similar in many respects to the small subunit clade 1 and clade 3 catalases.

EXPERIMENTAL PROCEDURES

Materials. BLC, proteinase K, and common biochemicals were obtained from Sigma Chemical Co. and Invitrogen. Catalase HPII was purified from transformed UM255 as previously described (*23*).

Enzyme and Protein Determinations. Catalase activity was determined by the method of Rørth and Jensen (*24*) in a Gilson oxygraph equipped with a Clark electrode. One unit of catalase is defined as the amount that decomposes 1 μmol of H_2O_2 in 1 min in a 60 mM H_2O_2 solution at pH 7.0 at 37 °C. The amount of protein was estimated according to the methods outlined by Layne (*25*). Absorption spectra were obtained using Milton Roy Spectronic 3000 and Pharmacia Ultrospec 4000 spectrophotometers. Unless otherwise indicated, samples were in 50 mM potassium phosphate (pH 7.0).

Conditions of Proteolysis. HPII and its His392Ala (*26*) variant were treated at 37 °C in 50 mM potassium phosphate (pH 7.0) with a 2:1 (w:w) ratio of HPII and proteinase K for 16 h. Proteolysis was stopped by the addition of phenylmethanesulfonyl fluoride (1 mM), and the mixture was fractionated by gel filtration on Superose 12 (Bio-Rad) (*22*).

Crystallization and Data Treatment. Crystals were obtained at room temperature by the vapor diffusion hanging drop method from 11.6 mg/mL protein, 50 mM Tris-HCl (pH 7.0), 8% PEG 20000, 8% PEG MME 550, 0.2 M KSCN, and 0.1 M dithiothreitol over the same reservoir solution. Crystals were monoclinic, in space group $P2_1$, with eight subunits or two tetramers in the crystal asymmetric unit.

Table 1: Data Collection and Structural Refinement Statistics for the Truncated HPII

data collection	
space group	$P2_1$
unit cell parameters	
a (Å)	111.0
b (Å)	152.9
c (Å)	135.3
α (deg)	90
β (deg)	97.5
γ (deg)	90
resolution (Å)	30−2.8 (2.8−2.87)[a]
no. of unique reflections	104927 (6917)[a]
completeness (%)	95.4 (92.1)[a]
R_{sym}[b]	0.106 (0.65)[a]
$\langle I/\sigma I\rangle$ (%)	6.6 (1.0)[a]
multiplicity	3.3 (3.0)[a]
model refinement	
no. of reflections	99638
R_{cryst} (%)[c]	21.7
R_{free} (%)[d]	26.9
no. of non-hydrogen atoms	31722
no. of water molecules	180
average B-factor (Å^2)	
protein	42.43
prosthetic group	35.41
waters	25.42
rms deviations	
bonds (Å)	0.019
angles (deg)	2.18

[a] Values in parentheses correspond to the highest-resolution shell. [b] $R_{sym} = \sum_{hkl}\sum_j|I_{hkl,j} - \langle I_{hkl}\rangle|/\sum_{hkl}\langle I_{hkl}\rangle$. [c] $R_{cryst} = \sum||F_{obs}| - |F_{calc}||/\sum|F_{obs}|$. [d] R_{free} is as for R_{cryst} but calculated for a test set comprising reflections not used in the refinement.

Diffraction data were obtained from crystals cooled with a nitrogen cryostream, giving the following unit cell parameters: $a = 111.0$ Å, $b = 152.9$ Å, $c = 135.3$ Å, $\alpha = \gamma = 90.0°$, and $\beta = 97.5°$. The diffraction data set was processed using MOSFLM (*27*) and scaled with SCALA (*28*); 5% of the measured reflections in every data set was reserved for R_{free} monitoring during automatic refinement (Table 1).

Structure determination was carried out with MOLREP (*29*) using HPII with the appropriate truncations to reflect the shorter sequence as the initial searching model. Refinements were completed using REFMAC (*30*) with solvent molecules modeled with WATPEAK (*26*) and manually with O (*31*). Solvent molecules were only introduced when they corresponded to the strongest peaks in the difference Fourier maps that could make at least one hydrogen bond with atoms already in the model. In the final rounds of refinement, the eight subunits were treated independently with the bulk solvent correction applied and the whole resolution range available used for each variant. The analysis of solvent accessibility and molecular cavities was carried out with VOIDOO (*32*) using a reduced atomic radius for polar atoms in accounting for possible hydrogen bonds (*26*). All figures were prepared using SETOR (*33*). Structure factors and coordinates have been submitted to the Protein Data Bank as entry 1YE9.

Mass Spectrometry. The protein was dialyzed into 5 mM ammonium acetate, and a 2 μM solution in that buffer was used for analysis of the pseudotetramer. Voltages were varied to assess the stability of the complex compared to a previous report on a different instrument (*22*). Partial denaturation was effected by preparing 2 μM protein in 0.5% acetic acid and 50% methanol, resulting in two envelopes of ions which

[1] Abbreviations: HPII, catalase from *E. coli*; BLC, bovine liver catalase; CATA, *S. cerevisiae* catalase A; PMC, *P. mirabilis* catalase; HEC, human erythrocyte catalase; MLC, *M. luteus* catalase; HPC, *H. pylori* catalase; PVC, *Pe. vitale* catalase; NCC, *N. crassa* catalase 1; EFC, *En. faecalis* catalase; rmsd, root-mean-square deviation.

could only be analyzed manually because of the complexity. All spectra were acquired by electrospray in a new time-of-flight instrument built at the University of Manitoba (*34*).

RESULTS

Physical Characterization of Truncated HPII. Treatment of HPII with proteinase K (2:1, w:w) for 16 h at 37 °C converts the 84 kDa subunits of the homotetramer into two fragments of approximately 26 and 32 kDa with predominant N-termini at Ser75 and Lys309, respectively (*22*). To better characterize the quaternary structure of the truncated enzyme, X-ray crystal structure refinement was pursued. Truncated HPII produced crystals that diffracted to 2.8 Å, yielding electron density maps that define an asymmetric unit containing eight subunits and eight heme groups organized in two tetramers. The subunits are actually pseudosubunits because each is composed of two fragments extending from Ser75 to Ala297 and Lys309 to Ile564 with no apparent density corresponding to the residues in the G_{298}-$KASLVWDEAQ_{308}$ sequence. The model has crystallographic agreement R and R_{free} factors of 21.7 and 26.9%, respectively, for 99 638 reflections in the resolution shell between 2.8 and 30.0 Å. The average rmsd after superimposition of the eight subunits is 0.09 Å for the Cα atoms and 0.23 Å for all atoms. As in the native enzyme, only Ile274, located adjacent to the beginning of the lateral channel, lies outside the energetically favorable regions in all subunits. The equivalent residues in all other catalases so far characterized (Val219 in CatF, Val238 in NCC, Val209 in PVC, Gly214 in CATA, Ser202 in MLC, Ser207 in HEC, Ser216 in BLC, Ser196 in PMC, Ser198 in HPC, and Ser196 in EFC) have a similar unusual conformation which enhances an intricate hydrogen bond network stabilizing the β-barrel core of the catalase subunit (*20*).

The folding of the two fragments in the pseudosubunit is very similar to the folding of the corresponding regions of an HPII subunit, with superimposition producing an average rmsd of 0.37 Å for 479 Cα atoms and 0.68 Å for all atoms. The greatest deviation is found in the surface loops of residues 510−523 and 551−564 with average rms deviations of 0.71 and 0.80 Å, respectively, for the Cα atoms (Figure 1). The greater movement of these segments can be attributed to the removal of residues 580−590 and 565−571 with which they normally interact. The truncated pseudosubunit also resembles the subunit of small subunit catalases with a shortened N-terminal arm (Ser75−Val127), the typical antiparallel eight-stranded β-barrel structure (His128−Phe391, albeit with a gap of Gly298−Gln308), an extended wrapping loop (His392−Tyr504), and a short helical domain at the carboxy terminus (Tyr505−Ile564) (Figure 1). As a result of the shortened N-terminus, only four residues protrude through the overlapping fold of the adjacent subunit, a length similar to that of small subunit catalases such as HPC.

The main access route for substrate H_2O_2 into the active site heme pocket is believed to be the main channel oriented perpendicular to the plane of the heme. In contrast to some small subunit enzymes, the additional protein sequence in the larger subunit HPII obstructs the channel, making it longer and narrower with a bifurcated entrance (Figure 2). In fact, the main contributor to the bifurcation and narrowing is a small six-residue insert, including Ser234 in the core of the protein, and the C-terminal domain does not significantly contribute to the constriction. Indeed, surface maps calculated in VOIDOO reveal that removal of the C-terminal domain leaves the opening to the main channel relatively unchanged compared to the native enzyme (Figure 2). By contrast, the opening of the lateral channel is significantly altered by the removal of the segment from residue 580 to 590 that is situated next to the opening in the native structure (Figure 2). The opening is enlarged such that adjacent to Glu362 it is 13.8 Å wide compared to only 7.2 Å in the native enzyme. In addition, its length is shortened to 16 Å from the heme to Glu362 compared to a length of 24 Å from the heme to Ile593.

Mass spectrometry analysis of the denatured enzyme identified two overlapping ion envelopes (Figure 3) consistent with there being some heterogeneity around the cleavage sites. The first envelope consisted of the 8+ to 11+ ions from a 25 kDa group of proteins, and the second consisted of the 9+ to 12+ ions from a 29 kDa group of proteins. The first group matched E76−K299, E76−A300, S75−K299, and S76−A300 (25 421, 25 492, 25 511 and 25 578 Da, respectively), and the second group matched K309−I564, L310−L566, K309−E565, K309−L566, and K309−T567 (29 692, 29 806, 29 821, 29 932, and 30 033 Da, respectively). Because residues G298, K299, A300, E565, L566, and T567 seem to be present in some proportion of the fragments on the basis of mass spectrometry, they must be sufficiently disordered that they do not appear in the electron density maps. The nondenatured protein complex is 225 000 Da (electrospray mass spectrometry data not shown and preliminary data from ref *22*), or 700−800 Da larger than what is predicted by the denatured fragments with heme, possibly a result of associated sodium ions and waters trapped in the channels, as has been observed for the GroEL complex which also has a central channel (*35*).

Enzymatic Characterization of Truncated HPII. As well as being resistant to thermal denaturation (*21*) and proteolyis (*22*), HPII begins to exhibit inhibition only at H_2O_2 concentrations above 3 M, whereas most small subunit catalases begin to exhibit inhibition between 300 mM and 1 M H_2O_2 (*36*). Truncated HPII is more sensitive to H_2O_2, closely resembling the most peroxide resistant small subunit enzymes in beginning to exhibit inhibition between 1 and 2 M H_2O_2 (Figure 4). At the same time, the turnover rate of the truncated enzyme is increased almost 2-fold, albeit at a much lower peroxide concentration, compared to that of the native enzyme, resulting in a specific activity 3.2 times higher than the native value (Table 2).

The Arg260Ala variant of HPII exhibits a 2.6 times higher specific activity (53 700 units/mg) than the native enzyme, a property attributed to an internal enlargement of the lateral channel (*35*). Truncation of HPII results in the side chain of Arg260, associated with the side chain of Glu270, being situated on the surface of the protein near, but not precisely in, the entrance to the lateral channel, and its removal in the truncated Arg260Ala variant protein did not result in a significant change in specific activity (53 900 units/mg). The Arg260Ala variant of HPII was also characterized by enhanced sensitivity to certain inhibitors, including azide, hydroxylamine, methyl and ethyl hydroxylamine, and a variety of sulfhydryl reagents (*37*), as a result of channel

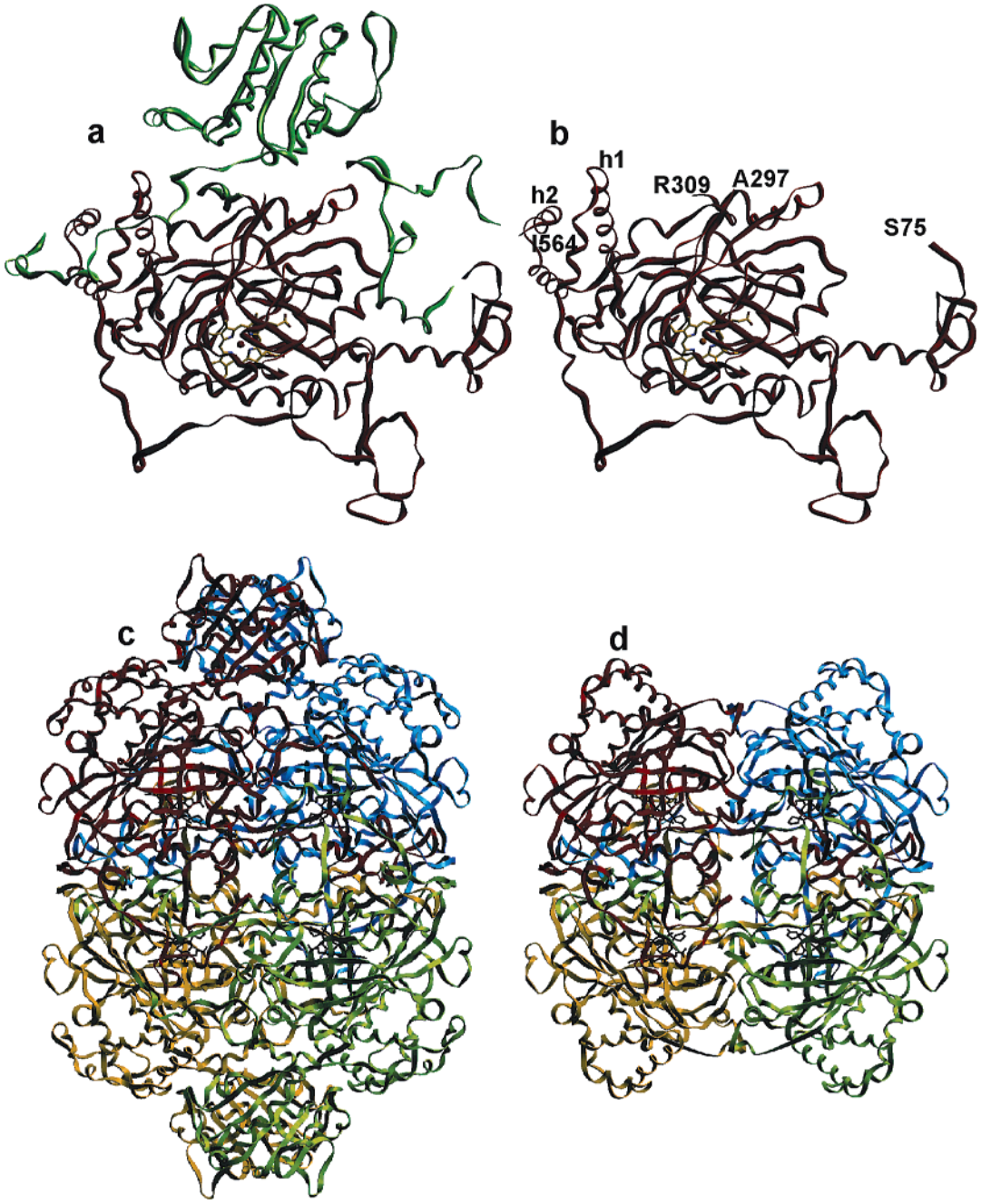

FIGURE 1: Comparison of the truncated variant of HPII with the native form and BLC. Single subunits are shown in panels a and b, and tetramers, looking down the P axis, are shown in panels c and d. Native HPII is shown in panels a and c; truncated HPII is shown in panels b and d. In panel a, the core of the subunit is colored red and the segments that are removed by proteolysis are shown as a heavier green ribbon. The two surface helices marked h1 (residues 510−523) and h2 (residues 551−546) exhibit a larger rmsd in comparison to the remainder of the molecule.

enlargement, and the truncated variant of HPII exhibits very similar properties. It is significantly more sensitive to both azide and aminotriazole, and slightly more sensitive to cyanide and hydroxylamine (Figure 5 and Table 2) compared to the native enzyme.

NADPH Binding and Compound II Formation. The absence of NADPH in native HPII is clearly attributable to a segment of the C-terminal domain, including residues 581−591, being folded into the binding pocket used in some small subunit enzymes, but there are also changes to two residues identified as being important for NADPH binding (*17*, *18*); Leu359 replaces Val, and Glu362 replaces His. The absence of residues 581−591 in truncated HPII presented the opportunity to determine if NADPH can bind despite the two residue changes. AffiBlue affinity gel for NADH-bound proteins could not be used because, unlike native HPII, truncated HPII surprisingly bound to the gel even in the absence of added NADPH. However, protein-associated fluorescence after incubation of the protein with NADPH and separation by gel filtration revealed NADPH association with BLC but not with either native [as reported previously (*38*)] or truncated HPII (data not shown).

Compound I of small subunit enzymes can suffer a one-electron reduction either with low concentrations of H_2O_2 or with potassium ferrocyanide to produce compound II. A similar pathway has been demonstrated in the heme *b*-containing large subunit catalase from *Aspergillus niger* (*39*), although compound II of this catalase was reduced more

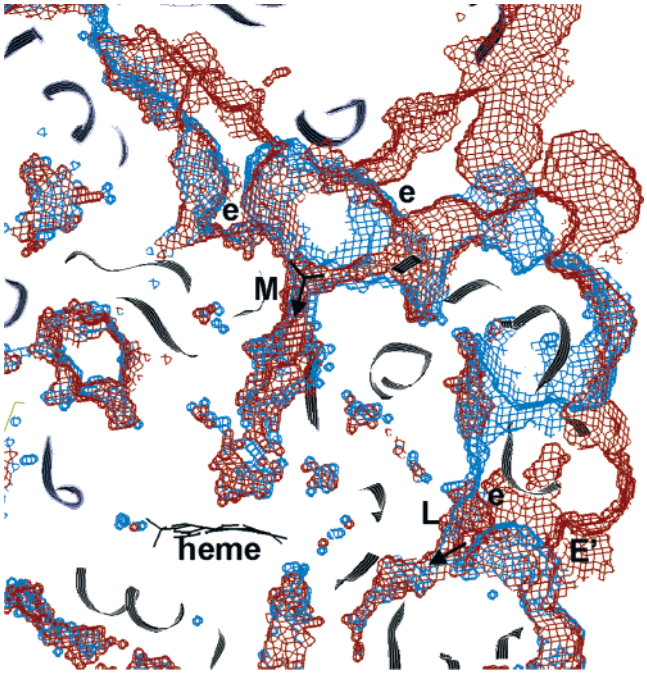

FIGURE 2: Surface maps of HPII (red) and the truncated variant (blue) in a slab encompassing the main (labeled M) and lateral (labeled L) channels leading to the heme pocket. The lowercase e indicates the entrance points to the channels in the truncated variant, and the uppercase E′ indicates the entrance to the lateral channel in the native enzyme. Note that the entrance points to the main channel do not change between the native and truncated enzymes. Arrows are superimposed on the channel, and in the main channel is intended to highlight the bifurcation in the channel.

rapidly back to a resting state than in the small subunit catalases. Compound II has not been observed in heme *d*-containing large subunit enzymes such as HPII (*40*), and to determine if this was because the extra protein sequence or the presence of heme *d* in HPII was affecting compound II formation, native and truncated HPII were incubated with a low concentration of H_2O_2 generated by glucose and glucose oxidase, revealing a hypochromic effect on both the Soret peak at 407 nm and the peak at 590 nm, but with no shift in peak location or appearance of new bands. By contrast, the spectral changes induced in BLC include a hypochromic red shift of the Soret band and the appearance of a new band at 570 nm (Figure 6) consistent with the formation of compound II (*1*, *39*). Peracetate treatment of truncated HPII elicits a hypochromic shift of both the Soret and 590 nm bands, an effect similar to that of low H_2O_2 concentrations, and subsequent addition of potassium ferrocyanide causes no further change (Figure 7a). The effect of peracetate and potassium ferrocyanide on native HPII was similar but not as pronounced (data not shown), presumably because of restricted access to the active site. In contrast to HPII and its truncated variant, BLC treated with peracetate produces a compound I-like spectrum, and subsequent treatment with potassium ferrocyanide converts it to a compound II-like spectrum (Figure 7c).

The conclusion that heme *d*-containing large subunit catalases do not form compound II is based on the absence of a compound II spectrum comparable to that generated in heme *b*-containing small and large subunit enzymes (Figures 6 and 7; *39*). However, because a heme *d* compound II spectrum is unknown, it remains a possibility that the spectra of compounds I and II in heme *d*-containing enzymes are

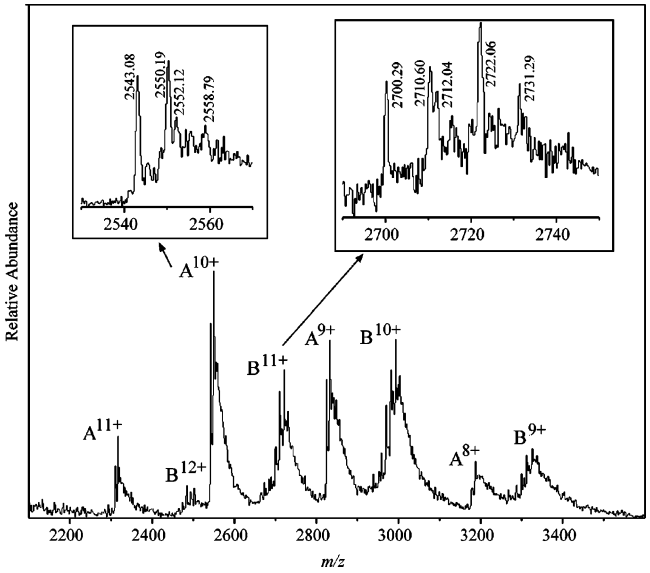

FIGURE 3: Part of the ESI-mass spectrum of the truncated HPII complex after acidification. Manual deconvolution of the A series ions (from expansion of the 10+ ion in the inset) matches the protein sequences of E76−K299 (measured, 25 421 Da; expected, 25 421.62 Da), E76−A300 (measured, 25 492 Da; expected, 25 492.70 Da), S75−K299 (measured, 25 511 Da; expected, 25 508.70 Da), and S75−A300 (measured, 25 578 Da; expected, 25 579.78 Da). Manual deconvolution of the B series ions (from expansion of the 11+ ion in the inset) matches the protein sequences of K309−I564 (measured, 29 692 Da; expected, 29 692.24 Da) L310−L566 (measured, 29 806 Da; expected, 29 806.34 Da), K309−E565 (measured, 29 821 Da; expected, 29 821.36 Da), K309−L566 (measured, 29 932 Da; expected, 29 934.52 Da), and K309−T567 (measured, 30 033 Da; expected, 30 035.62 Da). Sodium adducts were also present, but are not labeled.

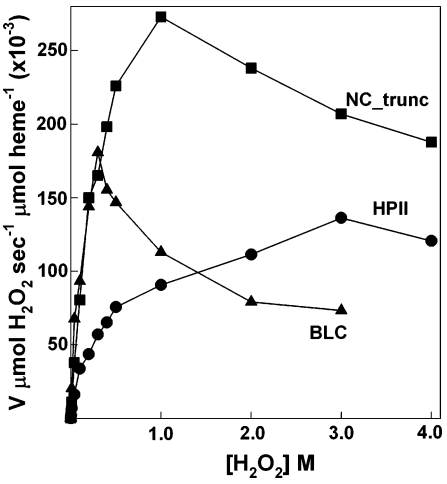

FIGURE 4: Comparison of the reaction velocities of native HPII (●) and its truncated variant (■) as a function of H_2O_2 concentration. The kinetics of BLC (▲) are included for comparison.

indistinguishable. Treatment of the heme *b*-containing His392Ala variant of HPII, truncated with proteinase K, with peracetate generates a typical heme *b* compound I spectrum, and subsequent treatment with potassium ferrocyanide generates a typical heme *b* compound II spectrum (Figure 7b), similar to that of *A. niger* catalase (*39*), confirming that the large subunit protein itself is not a block to compound II formation. Longer incubation of truncated HPII and the truncated His392Ala variant with potassium ferrocyanide results in spectral changes consistent with regeneration of the resting state (Figure 8a,b), in contrast to BLC for which

Table 2: Kinetic Parameters of HPII and Its Truncated Variant

	HPII	truncated HPII
k_{cat} (s^{-1})	151000 ± 8000	273000 ± 14000
$[H_2O_2]$ at $^1/_2V_{max}$ (mM)	312 ± 11	185 ± 8
SA (units/mg of protein)	20700 ± 400	64400 ± 700
[NaCN] at 50% inhibition (μM)	9 ± 0.3	6 ± 0.4
$[NaN_3]$ at 50% inhibition (μM)	130 ± 5	4 ± 0.3
$[NH_2OH]$ at 50% inhibition (μM)	0.12 ± 0.01	0.08 ± 0.01
[aminotriazole] at 50% inhibition (mM)	>1000	300 ± 20

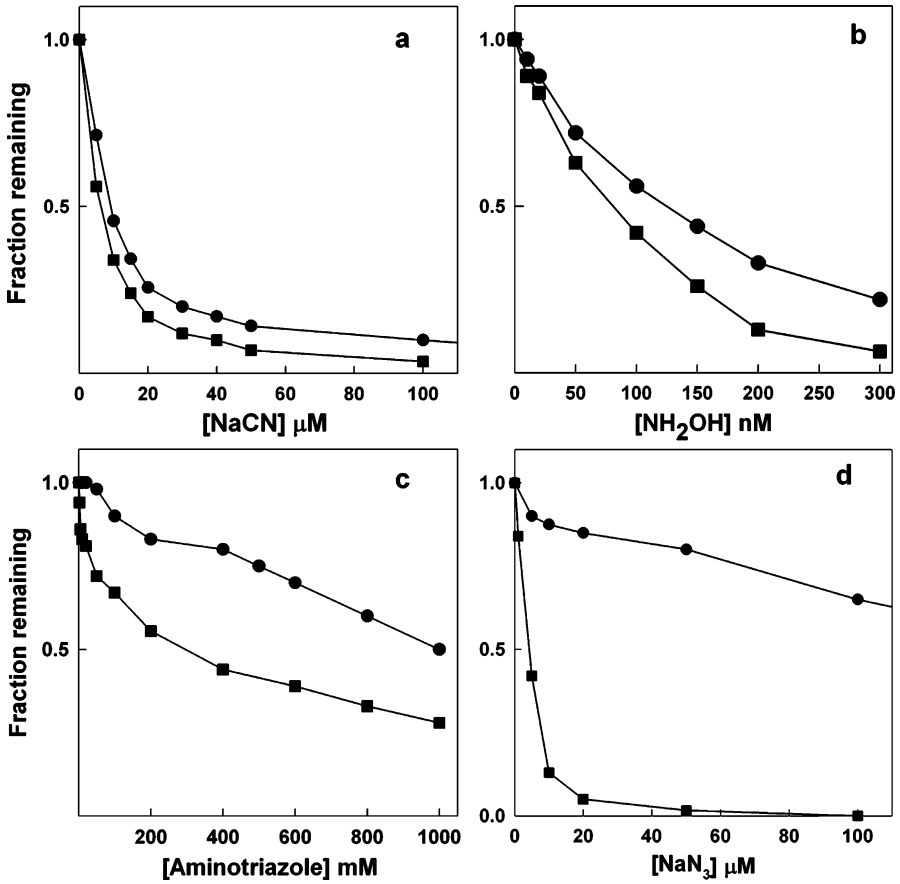

FIGURE 5: Inhibition of native HPII (●) and its truncated variant (■) by NaCN (a), NH_2OH (b), aminotriazole (c), and NaN_3 (d). The enzymes were incubated with the inhibitor for 1 min before initiation of the catalase assay.

the spectrum remains compound II-like in the 500−700 nm region, albeit with a Soret band gradually increasing in magnitude (Figure 8c).

DISCUSSION

A detailed phylogenetic analysis of catalases had previously concluded that the progenitor catalase may have been a large subunit enzyme from which the small subunit enzymes evolved (*3*). The current demonstration that a large subunit catalase can be truncated by proteolysis to a form that closely resembles a small subunit catalase confirms that a conversion from large to small is indeed possible. Obviously, evolution would have involved gene truncation, and previous attempts to truncate *katE* had revealed that removal of parts of the gene encoding any N-terminal residues and more than nine C-terminal residues (I745−A753) sufficiently interfered with folding that proteolysis was able to significantly reduce the level of protein accumulation (*41*). Clearly, mutations that facilitate folding of the truncated protein must have accompanied the gene truncation events, or the progenitor catalase did not suffer the same folding problems upon truncation. The fact that only a small number of nonpolar side chains in each subunit become exposed on the surface as a result of the truncation, including Ile262, Leu310, Phe317, Phe518, and Phe529, and that a similar number of polar side chains are exposed, including T268, R264, D321, E324, H522, and K533, may explain why the enzyme remains soluble after such extensive truncation.

Successful purification and crystallization of the extensively proteolyzed HPII reinforces the image of HPII, and catalases in general, as very robust enzymes. In its native state, HPII resists thermal inactivation to more than 80 °C and does not exhibit inhibition even in 3 M H_2O_2 solutions. The truncated protein created by removal of the N- and C-terminal domains has properties more similar to those of small subunit enzymes, including a faster turnover rate, a temperature of thermal inactivation lowered to 59 °C, and increased sensitivity to peroxide with inactivation becoming evident above 1 M H_2O_2. Therefore, the additional 274 residues in the N- and C-terminal regions impart relatively

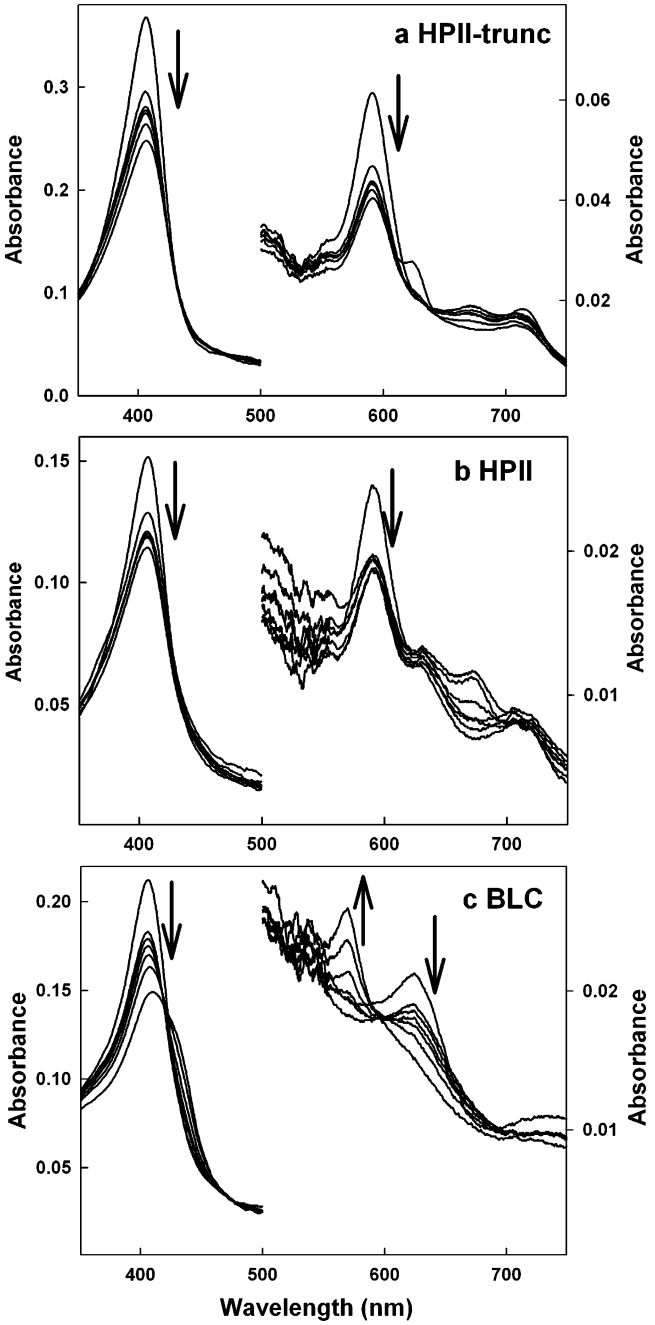

FIGURE 6: Changes in absorbance spectra of truncated HPII (a) and native HPII (b) and BLC (c). Scans were taken 0, 0.5, 2.5, 5, 10, 20, 30, and 60 min after the addition of 4 mM glucose to a solution of 4 μM enzyme and 5 nM glucose oxidase in 10 mM potassium phosphate (pH 6.5). The arrows adjacent to or above or below the main peaks indicate the trend of changes in that peak. The left axis corresponds to 350−500 nm, and the right axis corresponds to 501−750 nm.

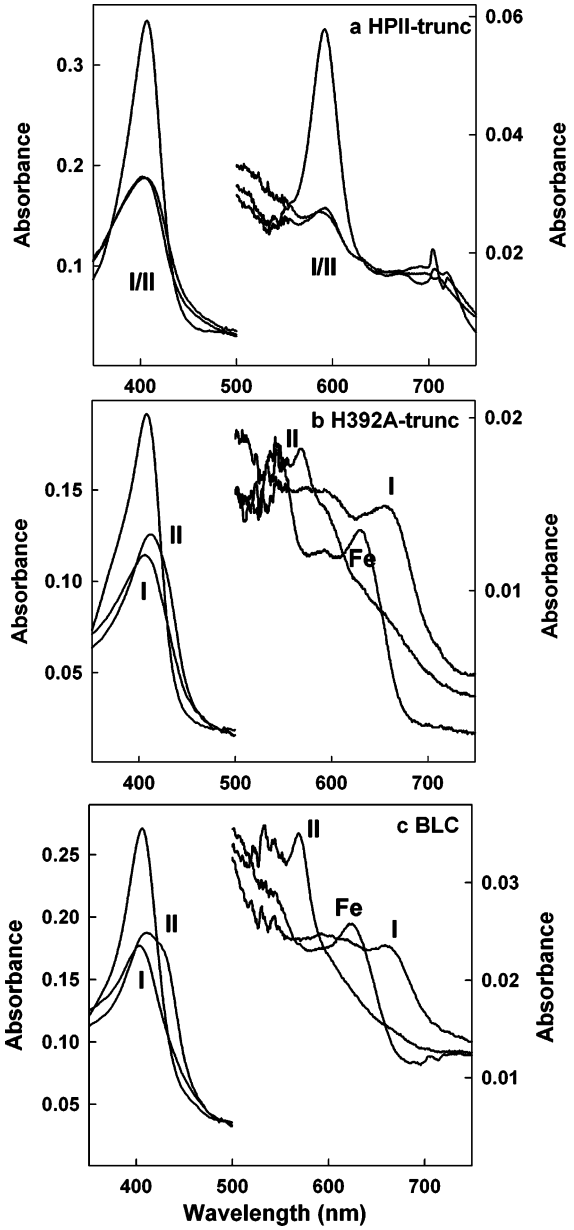

FIGURE 7: Changes in absorbance spectra of truncated HPII (a), the truncated His392Ala variant of HPII (b), and BLC (c). Each panel contains a spectrum of 4 μM untreated enzyme in 10 mM potassium phosphate (pH 7.0) (labeled Fe), a spectrum of the same enzyme 1 min after mixing with 6 μM peracetate (labeled I), and the same mixture 10 min after the addition of 8 μM potassium ferrocyanide (labeled II). The left axis corresponds to 350−500 nm, and the right axis corresponds to 501−750 nm.

subtle changes to the properties of the 479 core residues, primarily involving enhanced stability or rigidity, and enhanced resistance to high peroxide concentrations.

The mechanisms by which the additional sequence causes these changed properties are similarly subtle. Enhanced resistance to higher peroxide concentrations and the slower turnover rate in large subunit catalases are best explained by more difficult access to the active site caused by occluded channels. The unusual stability of the dimer, separable only at temperatures above 95 °C, was originally ascribed to the "Velcro strap" arrangement of 80 N-terminal residues inserted through a loop on an adjacent subunit and folded back to interact with other parts of its own subunit (*21*). However, removal of 75 N-terminal residues caused only a minor reduction in the thermal stability of the enzyme, whereas removal of the 150-residue C-terminal domain reduced thermal stability by almost 25 °C (*22*). This was unexpected because almost all of the C-terminal interactions are with other parts of its own subunit rather than with adjacent subunits, and it suggests that the role of the C-terminal domain lies in an enhancement of the intrinsic stability and rigidity of individual subunits which stabilizes subunit−subunit interactions.

The role ascribed to NADPH bound to a subset of catalases, including BLC and some other clade 3 catalases,

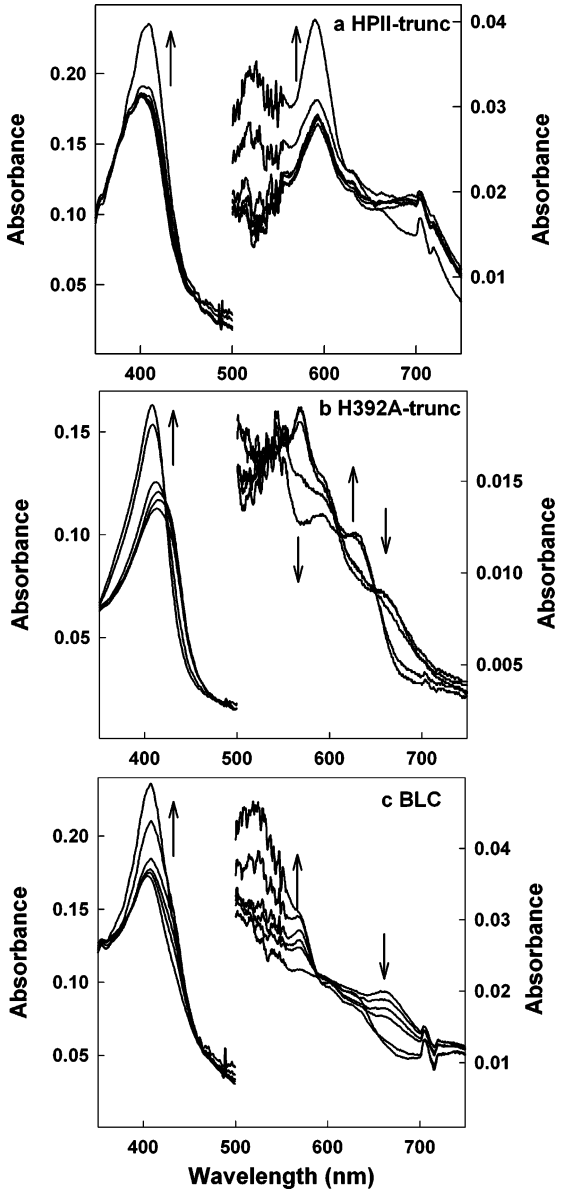

FIGURE 8: Absorbance spectra of the same samples described in the legend of Figure 7 taken 2, 5, 10, 20, and 60 min after the addition of potassium ferrocyanide. The arrows adjacent to or above or below the main peaks indicate the trend of changes in that peak. The left axis corresponds to 350−500 nm, and the right axis corresponds to 501−750 nm.

but not large subunit catalases, is the prevention of compound II formation, thereby preventing the gradual inactivation of catalase at low peroxide concentrations (*40*, *42*−*44*). The correlation between the absence of NADPH binding to large subunit enzymes and the lack of compound II formation has been noted (*40*). Clade 2 large subunit and clade 1 small subunit catalases do not bind NADPH, demonstrating that it is not needed to prevent compound II accumulation in all catalases. In the case of heme *d*-containing enzymes such as HPII and its truncated variant, there is no spectral evidence that a unique one-electron reduction product of compound I, such as compound II, is formed. However, the heme *b*-containing *A. niger* catalase and the truncated His392Ala variant of HPII can be converted transiently to a species with a compound II-like spectrum, demonstrating that compound II can be formed in the large subunit enzymes. More significantly, the reduction of compound I of the large subunit enzymes through compound II to a resting state occurs at approximately the same rate as the reduction of compound I of heme *d*-containing HPII back to a resting state. An EPR analysis which presents a paramagnetic compound I and an EPR silent compound II may shed some light on whether the spectra of heme *d* compound I and II species are indistinguishable or if the compound II intermediate is reduced so rapidly that it does not accumulate. It is clear that binding of NADPH to HPII is not needed because, even if compound II is formed, it is reduced to a resting state and does not accumulate as an inactive species.

REFERENCES

1. Nicholls, P., Fita, I., and Loewen, P. C. (2001) Enzymology and structure of catalases, *Adv. Inorg. Chem. 51*, 51−106.
2. Klotz, M. G., Klassen, G. R., and Loewen, P. C. (1997) Phylogenetic relationships among prokaryotic and eukaryotic catalases, *Mol. Biol. Evol. 14*, 951.
3. Klotz, M. G., and Loewen, P. C. (2003) The molecular evolution of catalatic hydroperoxidases: Evidence for multiple lateral transfer of genes between prokaryota and from bacteria into eukaryota, *Mol. Biol. Evol. 20*, 1098−1112.
4. Murthy, M. R. N., Reid, T. J., Sicignano, A., Tanaka, N., and Rossmann, M. G. (1981) Structure of beef liver catalase, *J. Mol. Biol. 152*, 465−499.
5. Fita, I., Silva, A. M., Murthy, M. R. N., and Rossmann, M. G. (1986) The refined structure of beef liver catalase at 2.5 Å resolution, *Acta Crystallogr. B42*, 497−515.
6. Vainshtein, B. K., Melik-Adamyan, W. R., Barynin, V. V., Vagin, A. A., and Grebenko, A. I. (1981) Three-dimensional structure of the enzyme catalase, *Nature 293*, 411−412.
7. Vainshtein, B. K., Melik-Adamyan, W. R., Barynin, V. V., Vagin, A. A., Grebenko, A. I., Borisov, V. V., Bartels, K. S., Fita, I., and Rossmann, M. G. (1986) Three-dimensional structure of catalase from *Penicillium vitale*, at 2.0 Å resolution, *J. Mol. Biol. 188*, 49−61.
8. Murshudov, G. N., Melik-Adamyan, W. R., Grebenko, A. I., Barynin, V. V., Vagin, A. A., Vainshtein, B. K., Dauter, Z., and Wilson, K. (1982) Three-dimensional structure of catalase from *Micrococcus lysodeikticus* at 1.5 Å resolution, *FEBS Lett. 312*, 127−131.
9. Gouet, P., Jouve, H. M., and Dideberg, O. (1995) Crystal structure of *Proteus mirabilis* PR catalase with and without bound NADPH, *J. Mol. Biol. 249*, 933−954.
10. Bravo, J., Verdaguer, N., Tormo, J., Betzel, C., Switala, J., Loewen, P. C., and Fita, I. (1995) Crystal structure of catalase HPII from *Escherichia coli*, *Structure 3*, 491−502.
11. Bravo, J., Maté, M. J., Schneider, T., Switala, J., Wilson, K., Loewen, P. C., and Fita, I. (1999) Structure of catalase HPII from *Escherichia coli* at 1.9 Å resolution, *Proteins 34*, 155−166.
12. Berthet, S., Nykyri, L., Bravo, J., Maté, M. J., Berthet-Colominas, C., Alzari, P. M., Koller, F., and Fita, I. (1997) Crystallization and preliminary structural analysis of catalase-A from *Saccharomyces cerevisiae*, *Protein Sci. 6*, 481−483.
13. Maté, M. J., Zamocky, M., Nykyri, L. M., Herzog, C., Alzari, P. M., Betzel, C., Koller, F., and Fita, I. (1999) Structure of catalase-A from *Saccharomyces cerevisiae*, *J. Mol. Biol. 286*, 135−139.
14. Ko, T.-P., Safo, M. K., Musayev, F. N., Di Salvo, M. L., Wang, C., Wu, S.-H., and Abraham, D. J. (1999) Structure of human erythrocyte catalase, *Acta Crystallogr. D56*, 241−245.
15. Putnam, C. D., Arvai, A. S., Bourne, Y., and Tainer, J. A. (1999) Active and inhibited human catalase structures: Ligand and NADPH binding and catalytic mechanism, *J. Mol. Biol. 296*, 295−309.
16. Carpena, X., Perez, R., Ochoa, W. F., Verdaguer, N., Klotz, M. G., Switala, J., Melik-Adamyan, W., Fita, I., and Loewen, P. C. (2001) Crystallization and preliminary X-ray analysis of clade I catalases from *Pseudomonas syringae* and *Listeria seeligeri*, *Acta Crystallogr. D57*, 1184−1186.
17. Carpena, X., Soriano, M., Klotz, M. G., Duckworth, H. W., Donald, L. J., Melik-Adamyan, W., Fita, I., and Loewen, P. C. (2003) Structure of the clade I catalase, CatF of *Pseudomonas syringae*, at 1.8 Å resolution, *Proteins 50*, 423−436.

18. Loewen, P. C., Carpena, X., Rovira, C., Ivancich, A., Perez-Luque, R., Haas, R., Odenbreit, S., Nicholls, P., and Fita, I. (2004) Structure of *Helicobacter pylori* catalase, with and without formic acid bound, at 1.6 Å resolution, *Biochemistry 43*, 3089−3103.
19. Diaz, A., Horjales, E., Rudiño-Piñera, E., Arreola, R., and Hansberg, W. (2004) Unusual Cys-Tyr covalent bond in a large catalase, *J. Mol. Biol. 342*, 971−985.
20. Håkansson, K. O., Brugna, M., and Tasse, L. (2004) The three-dimensional structure of catalase from *Enterococcus faecalis*, *Acta Crystallogr. D60*, 1374−1380.
21. Switala, J., O'Neil, J. O., and Loewen, P. C. (1999) Catalase HPII from *Escherichia coli* exhibits enhanced resistance to denaturation, *Biochemistry 38*, 3895−3901.
22. Chelikani, P., Donald, L. J., Duckworth, H. W., and Loewen, P. C. (2003) Hydroperoxidase II of *Escherichia coli* exhibits enhanced resistance to proteolytic cleavage compared to other catalases, *Biochemistry 42*, 5729−5735.
23. Loewen, P. C., and Switala, J. (1986) Purification and characterization of catalase HPII from *Escherichia coli* K12, *Biochem. Cell Biol. 64*, 638−646.
24. Rørth, M., and Jensen, P. K. (1967) Determination of catalase activity by means of the Clark electrode, *Biochim. Biophys. Acta 139*, 171−173.
25. Layne, E. (1957) Spectrophotometric and turbidimetric methods for measuring proteins, *Methods Enzymol. 3*, 447−454.
26. Maté, M. J., Sevinc, M. S., Hu, B., Bujons, J., Bravo, J., Switala, J., Ens, W., Loewen, P. C., and Fita, I. (1999) Mutants that later the covalent structure of catalase hydroperoxidase II from *Escherichia coli*, *J. Biol. Chem. 274*, 27717−27725.
27. Collaborative Computational Project, Number 4 (1994) The CCP4 Suite: Programs for Protein Crystallography, *Acta Crystallogr. A50*, 760−763.
28. Evans, P. R. (1997) Scala, *Joint CCP4 and ESF-EACBM Newsletter 33*, 22−24.
29. Vagin, A., and Teplyakov, A. (1997) MOLREP: An automated program for molecular replacement, *J. Appl. Crystallogr. 30*, 1022−1025.
30. Murshudov, G. N., Vagin, A. A., and Dodson, E. J. (1997) Refinement of macromolecular structures by the maximum-likelihood method, *Acta Crystallogr. D53*, 240−255.
31. Jones, T. A., Zou, J. Y., Cowan, S. W., and Kjeldgaard, M. (1991) Improved methods for building protein models in electron density maps, *Acta Crystallogr. A47*, 110−119.
32. Kleywegt, G. J., and Jones, T. A. (1994) Detection, delineation, measurement and display of cavities in macromolecule structures, *Acta Crystallogr. D50*, 178−185.
33. Evans, S. (1993) SETOR: Hardware lighted three-dimensional solid model representations of macromolecules, *J. Mol. Graphics 11*, 134−138.
34. Kozlovski, V. I., Donald, L. J., Montero-Callado, V., Spicer, V., Loboda, A. V., Chernushevich, I. V., McNabb, J., Ens, W., and Standing, K. G. (2004) Studies of noncovalent complexes of citrate synthase and catalase on a new TOF mass spectrometer with an ESI source, orthogonal injection, and 16 kV acceleration voltage, Desorption 2004, St. Petersburg, Russia, Aug 29−Sept 2.
35. Rostom, A. A., and Robinson, C. V. (1999) Detection of the intact GroEL chaperonin assembly by mass spectrometry, *J. Am. Chem. Soc. 121*, 4718−4719.
36. Sevinc, M. S., Maté, M. J., Switala, J., Fita, I., and Loewen, P. C. (1999) Role of the lateral channel in catalase HPII of *Escherichia coli*, *Protein Sci. 8*, 490−498.
37. Switala, J., and Loewen, P. C. (2002) Diversity of properties among catalases, *Arch. Biochem. Biophys. 401*, 145−154.
38. Hillar, A., Nicholls, P., Switala, J., and Loewen, P. C. (1994) NADPH binding and control of catalase compound II formation: Comparison of bovine, yeast and *Escherichia coli* enzymes, *Biochem. J. 300*, 531−539.
39. Lardinois, O. M., and Rouxhet, P. G. (1994) Characterization of hydrogen peroxide and superoxide degrading pathways of *Aspergillus niger* catalase: A steady-state analysis, *Free Radical Res. 20*, 29−50.
40. Obinger, C., Maj, M., Nicholls, P., and Loewen, P. C. (1997) Activity, peroxide compound formation, and heme d synthesis in *Escherichia coli* HPII catalase, *Arch. Biochem. Biophys. 342*, 58−67.
41. Sevinc, M. S., Switala, J., Bravo, J., Fita, I., and Loewen, P. C. (1998) Truncation and heme pocket mutation reduce production of functional catalase HPII in *Escherichia coli*, *Protein Eng. 11*, 549−555.
42. Kirkman, H. N., and Gaetani, G. F. (1984) Catalase, a tetrameric enzyme with four tightly bound molecules of NADPH, *Proc. Natl. Acad. Sci. U.S.A. 81*, 4343−4347.
43. Kirkman, H. N., Galiano, S., and Gaetani, G. (1987) The function of catalase-bound NADPH, *J. Biol. Chem. 262*, 660−666.
44. Hillar, A., and Nicholls, P. (1992) A mechanism for NADPH inhibition of catalase compound II formation, *FEBS Lett. 314*, 179−182.
45. Obinger, C., Maj, M., Nicholls, P., and Loewen, P. C. (1997) Activity, peroxide compound formation, and heme d synthesis in *Escherichia coli* HPII catalase, *Arch. Biochem. Biophys. 342*, 58−67.

BI047277M